

Fuzzy Spectral and Spatial Feature Integration for Classification of Non-ferrous Materials in Hyper-spectral Data

Artzai Picón, Ovidiu Ghita, Paul F. Whelan, *Senior Member, IEEE*, and Pedro M^a Iriondo

Abstract— Hyper-spectral data allows the construction of more elaborate models to sample the properties of the non-ferrous materials than the standard RGB color representation. In this paper, the non ferrous waste materials are studied as they cannot be sorted by classical procedures due to their color, weight and shape similarities. The experimental results presented in this paper reveal that factors such as the various levels of oxidization of the waste materials and the slight differences in their chemical composition preclude the use of the spectral features in a simplistic manner for robust material classification. To address these problems, the proposed FUSSE (FUZZY Spectral and Spatial classifiER) algorithm detailed in this paper merges the spectral and spatial features to obtain a combined feature vector that is able to better sample the properties of the non ferrous materials than the single pixel spectral features when applied to the construction of Multivariate Gaussian Distributions. This approach allows the implementation of statistical region merging techniques in order to increase the performance of the classification process. To achieve an efficient implementation, the dimensionality of the hyper-spectral data is reduced by constructing bio-inspired spectral fuzzysets that minimize the amount of redundant information contained in adjacent hyper-spectral bands. The experimental results indicate that the proposed algorithm increased the overall classification rate from 44% using RGB data up to 98% when the spectral-spatial features are used for non-ferrous material classification.

Index Terms—Hyper-spectral image processing, spectral fuzzysets, image classification.

I. INTRODUCTION

NOWADAYS, sustainable development has become one of the most important paradigms of the contemporary

Manuscript received April 21, 2009. This work was supported in part by the Etorrek program of the Basque Government.

A. Picón is with the Infotech Unit of the Tecnalia Research Corporation, Zamudio, Bizkaia, SPAIN (e-mail: apicon@robotiker.es).

O. Ghita is with the Centre for Image Processing and Analysis, School of Electronic Engineering, Dublin City University, IRELAND. (e-mail: ghita@eeng.dcu.ie).

P. F. Whelan is with the Centre for Image Processing and Analysis, School of Electronic Engineering, Dublin City University, IRELAND. (e-mail: paul.whelan@dcu.ie).

P. Iriondo is with the Department of Automatic Control and Systems Engineering, ETSI of Bilbao, University of the Basque Country UPV-EHU, SPAIN (e-mail: pedro.iriondo@ehu.es).

societies since a large amount of electrical and electronic equipment is being designed, manufactured and retired. Thus, the problem of processing and recycling the electrical and electronic waste is of paramount importance since this type of waste is not bio-degradable and may be contaminated with highly toxic substances.

Currently, the recycling process is carried out in generic dumps where the electronic waste is mixed among other waste materials. While a wide variety of materials are used to manufacture the electrical and electronic products, the process required to recycle the Waste from Electrical and Electronic Equipment (WEEE) is one of the most complex and labor intensive industrial tasks.

In recent years, due to the environmental legislation that has been introduced in regard to the recycling process for WEEE, the development of systems that are able to sort and process the electrical and electronic waste in an automatic fashion has been viewed as the most cost-effective recycling solution. For instance, the EC WEEE Recycling Directive [1] states that all EU countries have to recover about 70-80% of the weight of the produced WEEE and to reuse 50-75% of the recovered materials or components. This law strengthened the necessity to devote additional efforts in the development of new techniques and technologies that are able to improve the performance of the methods that are currently applied for WEEE recycling.

After the WEEE scrap is subjected to shredding, magnetic, mechanical and densiometric sorting, the resulting waste fractions still contain a mix of non-ferrous metals (e.g. aluminum, copper, zinc, brass, and lead) and austenitic Stainless Steel representing approximately 13% of the total WEEE weight. It is important to mention that the non-ferrous and austenitic Stainless Steel cannot be identified and separated using the current recycling methods [2], [3].

As the price of the recycled materials depends largely on purity, the non-ferrous fractions resulting after WEEE recycling are currently sold at a much lower price and their reutilization is more difficult. A proper separation of these non-ferrous metals will allow a substantial increase in the added value of the whole recycling process and helping the EU countries to comply with the 2002/96/EC directive.



Fig. 1. Fractions of different non-ferrous metals and Stainless Steel resulting from the WEEE recycling process.

The methods that are currently applied to separate the non-ferrous metals and Stainless Steel involve a visual inspection based on the color properties associated with the analyzed materials [4]. In this regard, Kutila et al [5] developed a color inspection system that was applied to separate the metals whose colors are predominantly red (brass, copper) from the bright metals such as Stainless Steel, aluminum and zinc. The experiments reported in their paper indicate that the materials defined by red properties can be separated from the materials with bright colors (reported classification accuracy 83.5%), but the results were inaccurate when they attempted to separate the metals with similar chromatic properties (the reported classification accuracies for materials such as copper and brass dropped to 37.4% and 36.8% respectively). X-Ray methods have been widely used for metal scrap and plastic sorting [6], [7]. However, the application of X-Ray backscatter imaging to tasks such as the sorting of non-ferrous materials in industrial environments may encounter difficulties as this technology only measures the material density [4]. The only methods that proved efficient in classifying non-ferrous metals are based on the analysis of the spectrum emitted by metals after they were subjected to thermal stress [8]. These methods cannot be used for recycling purposes due to the low speed of the spectrum acquisition process and the technical difficulties to devise a suitable excitation method for each WEEE non-ferrous fraction.

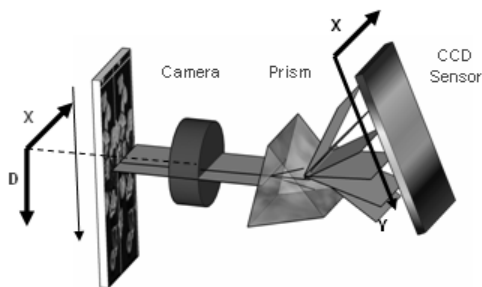


Fig. 2. The hyper-spectral image acquisition process.

Modern optical spectrometers overcome these problems as they provide high-resolution spatial image data with a detailed spectral accuracy. This technology involves the capture and interpretation of multi-dimensional digital

images and the current range of spectral imaging systems is able to capture multiple bands from ultraviolet to far infrared with good bandwidth resolution. This versatility enables the application of the spectral imaging systems in the detection and classification of various natural and man-made materials such as minerals, metals, plastic, vegetation, etc. [7], [9-11]. Recently, spectral data has been used to model the characteristics of the human tissues when applied to the development of robust face discriminators [12] and to properly characterize welding defects using a hybrid neural network-fuzzy-logic approach [13].

A characteristic of the hyper-spectral images is that each pixel is defined by a vector whose elements are the different spectral (wavelengths) components captured from the scene. This hyper-spectral vector provides not only the color information associated with the scene, but also information in regard to the chemical composition of the scene materials [9], [14-16].

To distinguish among different spectrums, several similarity measures were proposed in the literature on hyper-spectral data analysis [17]. The classical approaches that evaluate the distances between various spectrums in the \mathbf{R}^n Euclidean space or those based on the measurement of the angle between spectrums' SAM (Spectral Angle Mapper) [18] offer a good estimation in regard to the similarity of two spectrums, but they do not analyze the correlation between the data contained in adjacent spectral bands [9]. Consequently, these approaches are not able to properly accommodate the intra-class variations that are generated by the spectral differences between samples that belong to the same material. (In the context of material classification the intra-class variations are caused by external factors including metal oxidization, non-uniform illumination conditions, specular highlights, shadows, etc.)

The intra-class variations can be appropriately modeled by the use of pattern recognition techniques since the spectral information is evaluated in a more elaborate fashion [15], [19]. One problem that has to be addressed is the high dimensionality of the hyper-spectral data [20-22]. In this sense, to circumvent the problems caused by the large resolution of the hyper-spectral data when used for classification purposes, feature reduction techniques are usually applied to avoid the Hughes phenomenon [23]. To this end, the information contained in the spectral bands can be either decorrelated using Principal Component Analysis (PCA) [20], Wavelet decomposition [24-26], or by applying user-defined band selection [22], [27], [28]. Once the hyper-spectral data is decorrelated, the feature vectors describing the spectrum are extracted and used for classification tasks. Typically, the feature vectors are constructed using the spectral information associated with each pixel in the image [29-31], but recent approaches suggested to merge the spectral and spatial information in order to increase the classification accuracy [32-34].

In this paper, we propose to use hyper-spectral data to separate different non-ferrous materials using feature vectors that sample the material characteristics in the spectral-spatial domain. This paper is organized as follows.

In Section II, an overview of the developed material classification system is detailed where the key issue is the application of the spectral fuzzysets for hyper-spectral data decorrelation. This approach uses the physical properties of the spectrums to overcome some of the limitations associated with other decorrelation methods such as Principal Component Analysis (PCA) and Linear Discriminant Analysis (LDA) among others. Building on this concept, spectral-spatial features are constructed to model the characteristics of the non-ferrous materials by the use of spatial fuzzy histograms. Sections III and IV detail the classification process and introduce the statistical region merging approach that is applied to join the connected regions with similar properties. Section V details the experimental results, while in Section VI concluding remarks are provided.

II. SYSTEM OVERVIEW

This section outlines the complete procedure that has been developed to extract the feature vectors from the acquired spectral images. Also, in this section we explain how the spectral-spatial features are used for non-ferrous material classification.

The proposed algorithm, called FUSSE (FUZZY Spectral and Spatial feature classifiER), can be divided into two main components. The first component, as illustrated in Fig. 3, performs the normalization and decorrelation of the spectrum and the spectral-spatial feature merging. The computational stages associated with the first component of the algorithm can be summarized as follows,

1. Image acquisition.
2. Data normalization.
3. Spectral decorrelation.
4. Spectral-spatial feature integration.
5. 1st Stage classification.

As illustrated in Fig. 3, the captured spectral image data is subjected to intensity normalization, filtering and decorrelation. Different decorrelation techniques such as PCA, LDA, Wavelet decomposition and the proposed spectral fuzzysets are analyzed in our study. This is followed by the calculation of the spectral-spatial features by constructing fuzzy histograms in pre-defined neighborhoods for each pixel in the decorrelated image data. Finally, the extracted feature vectors are fed into the first stage classifier which creates an initial partition of the image with respect to the materials contained in the image data.

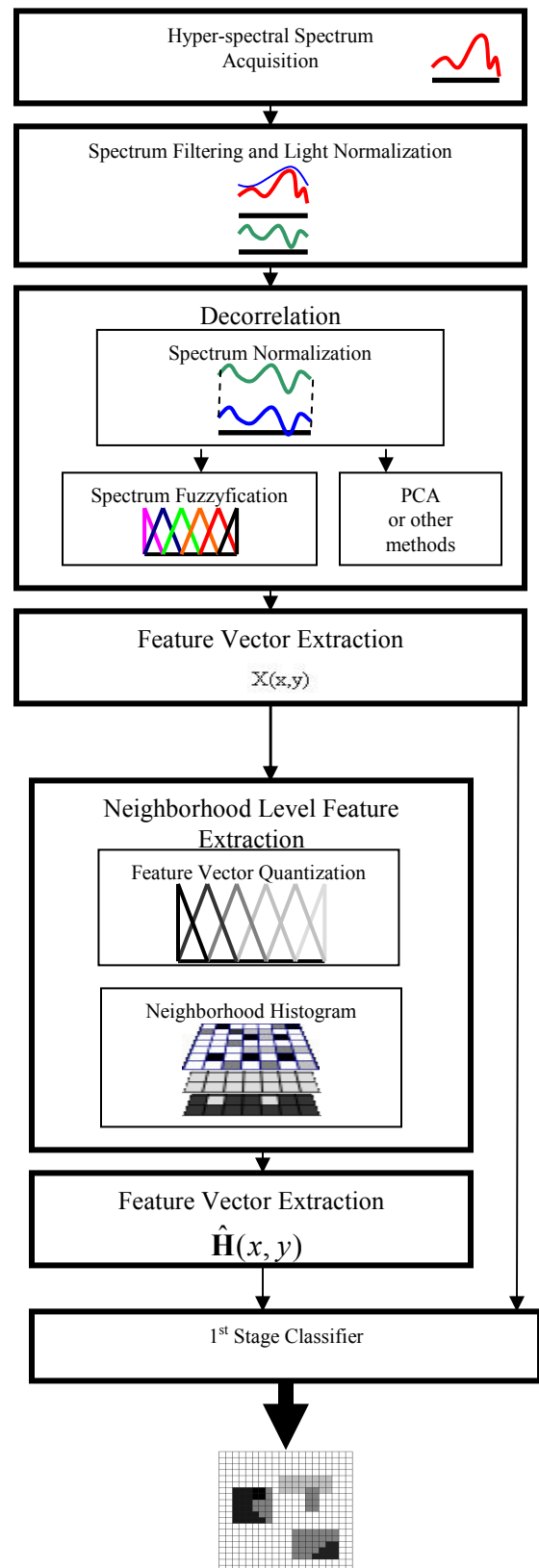


Fig. 3. Outline of the first component of the FUSSE algorithm.

The second component of the developed algorithm, as illustrated in Fig. 4, implements a statistical re-classification and region merging approach that is applied to refine the initial partition of the image resulting from the first component (see Fig. 3) of the material classification algorithm.

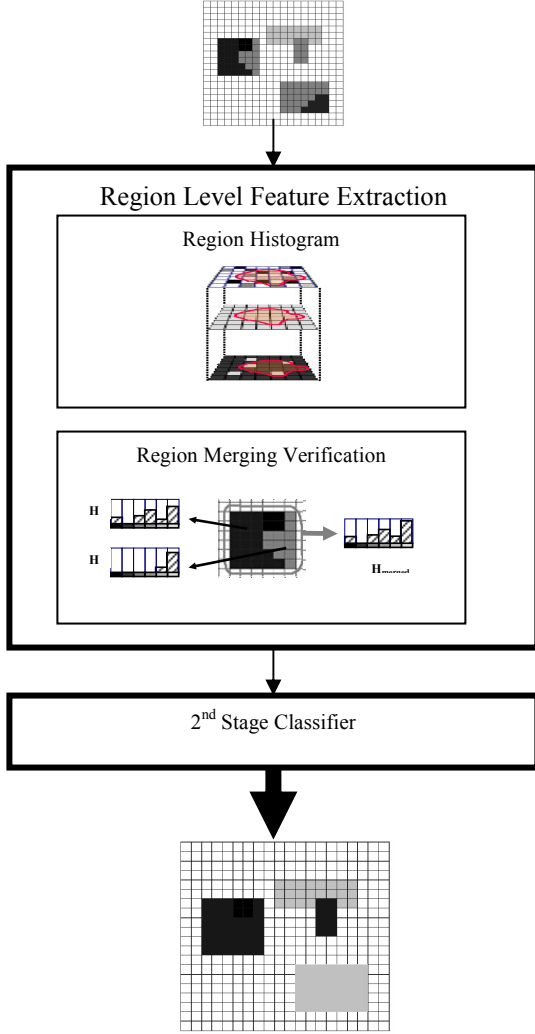


Fig. 4. Outline of the second component of the FUSSE algorithm.

A. Image Acquisition and Light Normalization

The acquired spectral data is represented by an image matrix where each element (pixel) at position (x, y) is represented by a vector \mathbf{L} . Let \mathbf{L} be the vector representation of the spectrum defined by the intensity responses of the K wavelengths and \mathbf{W} and \mathbf{B} be the vectors representing the white and black references of the spectrum as illustrated in Fig. 5.

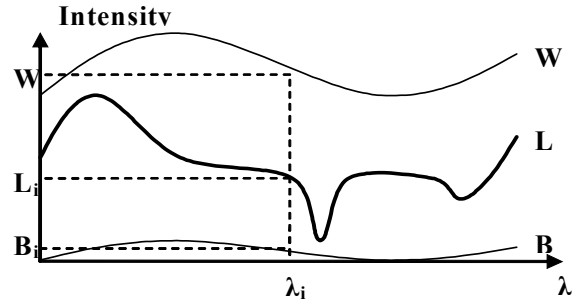


Fig. 5. Hyper-spectral vector (\mathbf{L}), white reference (\mathbf{W}) and black reference (\mathbf{B}) of the spectrum.

$$\mathbf{L} = \{L_1, L_2, \dots, L_K\}^T \quad (1)$$

$$\mathbf{W} = \{W_1, W_2, \dots, W_K\}^T \quad (2)$$

$$\mathbf{B} = \{B_1, B_2, \dots, B_K\}^T \quad (3)$$

In order to make the spectral vector \mathbf{L} independent to the illumination source, a solution is to normalize the hyper-spectral data using a dichromatic model such as that proposed by Shafer [35]. Shafer's illumination model assumes that the white illumination reference is known, but this approach is difficult to be directly applied to the normalization of the hyper-spectral data due to the complications associated with the development of a light source that has the same emittance for each wavelength. To be able to implement the Shafer's model when dealing with non-white hyper-spectral illumination, in our implementation we have adopted the approach proposed by Tan et al [36]. In this approach, the spectral components of the incident light are calculated at each location as illustrated in equation (4) and the spectrum is normalized using equation (5).

$$C_{light}(\lambda_i) = \frac{L_{light}(\lambda_i)}{\sum_{j=1}^k L_{light}(\lambda_j)} \quad (4)$$

$$\hat{L}(\lambda_i) = \frac{L(\lambda_i)}{C_{light}(\lambda_i)} \quad (5)$$

Since $L_{light}(\lambda)$ is not known for each pixel in the hyper-spectral data, the spectrum normalization will be indirectly performed using the reflections of the white (\mathbf{W}) and black reference (\mathbf{B}) as follows,

$$\hat{L}(\lambda_i) = \frac{L(\lambda_i) - B}{W - B} \quad (6)$$

Geusebroek et al [29] demonstrated that the highlights and shadows caused by the object geometry, material reflectance and position of the light source can be compensated for by applying intensity normalization and desaturation. Using this concept, in our implementation

each spectrum is first normalized by its mean and afterwards it is desaturated by the subtraction of its minimum value (7), as a variation of the method proposed by Stockman to extract the Spectral hue [37].

$$L_{norm}(\lambda_j) = L_N(\lambda_j) - \min_{i \in [1, k]} (L_N(\lambda_i)) \quad (7)$$

where $L_N(\lambda_j) = \frac{\hat{L}(\lambda_j)}{\sum_{m=1}^k \hat{L}(\lambda_m)}$ and $j \in [1, k]$.

B. Spectral Decorrelation

Since the hyper-spectral data is high dimensional and is characterized by a high level of redundancy, there is a significant overlap between the spectral distributions associated with different non-ferrous materials. In order to reduce the level of redundancy in the hyper-spectral data and improve the material separation, decorrelation techniques are applied to obtain a new data representation that has a reduced dimensionality. In this study different decorrelation methods are investigated, namely the Principal Component Analysis (PCA)-based approach [20], [26], Linear Discriminant Analysis (LDA) [19], [43], automatic band selection [47], Wavelet decomposition [25] and a novel technique based on spectral fuzzyfication that will be detailed in this paper.

PCA allows the extraction of highly discriminative features by performing an orthogonal decomposition of the hyper-spectral data. The main disadvantage associated with the PCA and related techniques such as LDA and Independent Component Analysis (ICA) [44] is that they require a training procedure that involves sampling relevant data-points from the high dimensional data. Another disadvantage of PCA resides in the fact that the compressed feature vectors are not directly linked with concrete physical variables and as a result they cannot be easily interpreted. Also, PCA requires retraining if new materials are included in the classification process.

To overcome the limitations associated with classical decorrelation techniques, a new method based on spectral fuzzyfication has been designed to optimize the discriminative power of the spectral features using an approach suggested by the human visual system when applied to the classification of non-ferrous materials.

B1. Classical Decorrelation Methodologies

The first decorrelation method analyzed in this paper is based on the widely used PCA (also referred in the computer vision literature to as Karhunen-Loève transform) technique [20], [38], [39]. PCA is a vector transform whose aim is to reduce the dimensionality of the input data by projecting it onto a lower dimensional orthogonal representation.

An adequate number of normalized vectors covering each class associated with non-ferrous materials are selected from training data in order to calculate the eigenvectors and

eigenvalues of their covariance matrix [39]. The first $M < K$ eigenvectors $\{\hat{\mathbf{u}}_1, \hat{\mathbf{u}}_2, \hat{\mathbf{u}}_3, \dots, \hat{\mathbf{u}}_M\}$ calculated from the covariance matrix are used to generate the transformation matrix \mathbf{V} . The PCA vector transform involves the projection of the high dimensional vectors on the transformation matrix \mathbf{V} as shown in equation (8).

$$\mathbf{X} = \mathbf{V}^t (\mathbf{L}_{norm} - \bar{\mathbf{L}}_{norm}) = [\hat{\mathbf{u}}_1, \hat{\mathbf{u}}_2, \hat{\mathbf{u}}_3, \dots, \hat{\mathbf{u}}_M]^T \cdot (\mathbf{L}_{norm} - \bar{\mathbf{L}}_{norm}) \quad (8)$$

where \mathbf{L}_{norm} is the normalized vector to be transformed, $\bar{\mathbf{L}}_{norm}$ is the mean vector of all normalized vectors selected for training and \mathbf{V} is the eigenmatrix defined by the first M eigenvectors calculated from the covariance matrix of the training vectors.

After the application of the PCA transformation, the spectrum is represented by \mathbf{X} vectors in the orthogonal PCA space. This representation offers a decorrelated and compressed version of the original hyper-spectral data that can be efficiently used for classification tasks. For comparative purposes, in this paper we also included the LDA, Wavelet and automatic band selection techniques to assess their performance when applied for data decorrelation.

B2. Spectral Fuzzysets

The method proposed in this paper to decorrelate the hyper-spectral data is based on the knowledge that the adjacent wavelengths of the spectrum are more correlated than the distant wavelengths. This observation is justified since for most solid materials the spectral information varies smoothly over successive spectral wavelengths [46]. Consequently, the spectral characteristics associated with non-ferrous materials are sampled by groups of adjacent spectral bands rather than unique spectral bands. To model this property, the intensity values for each wavelength have to take into account the values of the adjacent wavelengths. This can be obtained by dividing the spectrum in separate groups to attain the desired spectral selectivity. To avoid the problems caused by a crisp division of the spectrum, in this paper a method based on the spectrum fuzzyfication is proposed. This involves the separation of the hyper-spectral data into a number of fuzzy groups where each group covers a range of wavelengths and the contribution of each wavelength is modeled by a membership function.

Let \mathbf{L}_{norm} be the K normalized components of the spectrum as defined in equation (7) and M be the number of fuzzysets in which the spectrum will be divided. A membership function is defined for each of the fuzzysets to characterize the membership for any wavelength in the spectrum to its related fuzzyset. For the sake of simplicity, in this implementation triangular shaped membership functions are used (for a systematic approach in regard to the construction of the fuzzy rules the reader is directed to [41], [42]). In this way, the membership value for each

point of the spectrum is defined by a triangular function that is defined as follows,

$$Mf_i(\lambda) = \begin{cases} 1 - \left| \frac{\lambda - \lambda_{Ci}}{D} \right|, & \lambda_{Ci} - D < \lambda < \lambda_{Ci} + D \\ 0, & \text{Otherwise} \end{cases} \quad (9)$$

where λ_{Ci} is the central wavelength value of the fuzzysset i and D defines the separation between two consecutive central wavelengths as shown in Fig. 6.

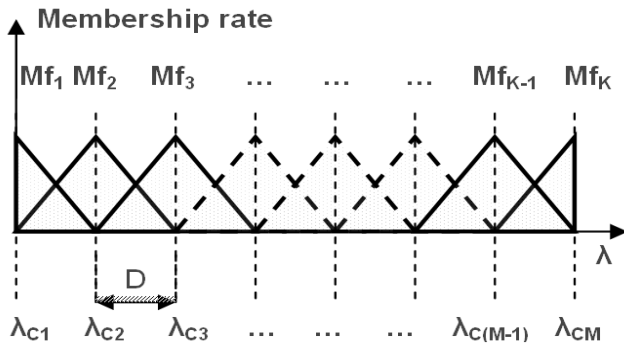


Fig. 6. Triangle shaped membership functions.

As illustrated in Fig. 6, each of the spectrum wavelengths has a membership grade to each of the segregated fuzzysets. In other words, each wavelength has a membership grade different than zero in the two adjacent groups and a membership grade of zero in the rest of the groups. This is shown in Fig. 7.

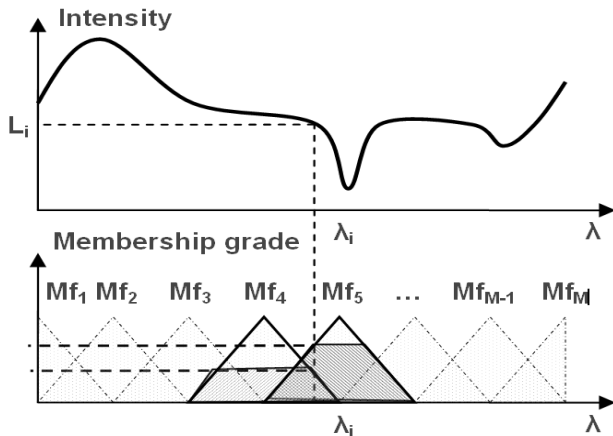


Fig. 7. An example that illustrates the membership grade associated with the wavelength λ_i .

The data resulting after the application of the fuzzysset representation to the initial hyper-spectral data is defined by the *Energy* of each fuzzysset that is calculated by weighting the intensity of each of the spectrum elements ($L_{norm}(\lambda_i)$) with the membership function associated with each fuzzysset as follows,

$$E_i = \int_{\lambda=0}^{\lambda=K} Mf_i(\lambda) \cdot L_{norm}(\lambda) d\lambda \quad (10)$$

The *Energy* measure defined in equation (10) samples the intensity of the spectrum in each of the fuzzysets. Based on the value of *Energy* for each fuzzysset, we can obtain useful information in regard to the radiometric (spectral) properties of the non-ferrous materials contained in the hyper-spectral image data. In this way, each hyper-spectral pixel is defined by a vector containing the *Energy* values of the M fuzzysets as illustrated in equation (11).

$$\mathbf{X} = \{E_1, E_2, \dots, E_M\}^T \quad (11)$$

This fuzzy representation allows us to characterize the spectral information in an efficient manner since the spectral features are not affected by the appropriate selection of the training elements as it is the case with the classical data decorrelation techniques. In addition, the dimensionality of the hyper-spectral data is optimally reduced since the fuzzyfication procedure maximizes the decorrelation between adjacent spectral bands, but at the same time maintains the physical meaning of the spectral features.

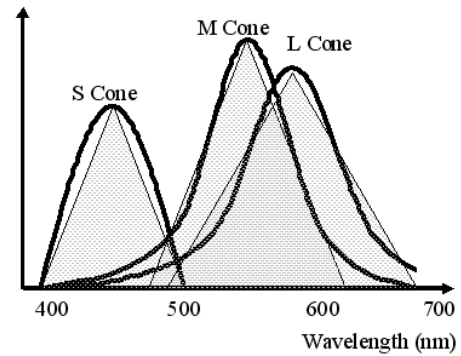


Fig. 8. Sensitivity of the human retinal receptors.

This approach is closely related to the way the human eye extracts the color information where each *Energy* value can be conceptualized as the amount of data absorbed by a color receptor (cone) present in the human visual system. The chromatic retinal receptors consist of three different types of cones, where each cell (cone) is able to convert the electromagnetic radiation emitted by the surface of the objects into chromatic information [46]. Each of these cones, as shown in Fig. 8, responds strongly to different parts of the spectrum (S=blue, M=green, L=red) and the colors sensed by humans are created as a combination of the three primary colors (R,G,B) given by the response of each type of cone. It is interesting to note that the chromatic receptors present in the human eye employ models that are consistent with the fuzzy set theory. Our approach based on the construction of spectral fuzzysets can be viewed as an extension of the process applied by the human vision system to attain the tri-chromatic information to the hyper-spectral case.

The decorrelated feature vectors defined in equation (11) contain only spectral information and they do not provide any spatial information (see Fig. 9).

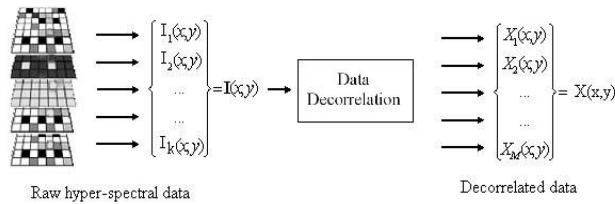


Fig. 9. Vectorial representation of the hyper-spectral image data.

Since the spatial information provides additional cues in characterizing the properties associated with non-ferrous materials, the development of a feature vector that encompasses the spatial and spectral information can increase the discrimination between different non-ferrous materials. To achieve this goal, fuzzy spatial histograms are proposed to merge the spectral and spatial features into a compound feature vector. These histograms encompass the distribution of the spectral vectors \mathbf{X} (see equations 8 and 11) in a given neighborhood or region.

C. Vector Quantization

Although the components X_i of the spectral vectors \mathbf{X} obtained after the application of the decorrelation techniques (based either on PCA or spectrum fuzzyfication) can be theoretically used to model the spectral properties of the non-ferrous materials, in practice they need to be quantized prior to the calculation of the feature histograms that integrate the spectral and spatial information. This approach is motivated by the fact that due to noise, various illumination conditions and various levels of oxidization, the spectral pixels that are sampled from same material very seldom have identical intensities values and these uncertainties between same-material pixels may cause severe classification errors.

The classical approach to calculate the spectral-spatial features involves the binning of the X_i values in a feature histogram that is calculated over a predefined neighbourhood in the image. This approach returns inappropriate results since the spectral components X_i show little variation among non-ferrous materials and the simplistic crisp binning process can induce erratic changes in the histograms if the intensity values of the X_i components are in the vicinity of the borders between bins. To address this issue we generate a normalized representation, where each component X_i of the spectral vectors \mathbf{X} is mapped into vector by the use of fuzzy membership functions. Using this approach, each spectral component X_i generates a quantized vector where the elements of the vector represent the grade of membership of the intensity value X_i with respect to the M fuzzysets that are applied to sample the hyper-spectral domain. The proposed fuzzy-based quantization procedure is illustrated in Fig. 10. This fuzzy-based representation has the advantage that the

variations between the spectral components X_i and the uncertainties caused by noise or different levels of material oxidization are better modeled than in the case when crisp binning would be employed.

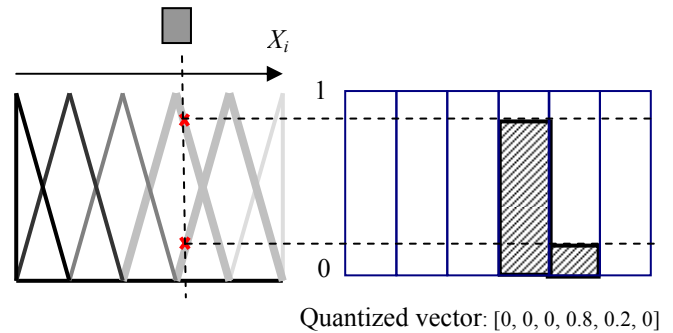


Fig. 10. The fuzzy-based vector quantization procedure. This diagram illustrates the calculation of the quantized vectors when 6 fuzzysets are employed to sample the hyper-spectral domain.

The quantization procedure shown in Fig. 10 is performed for each component of the spectral pixel and the quantization vector $\mathbf{Q}(x,y)$ is created by concatenating the quantization vectors resulting from each component X_i of the spectral vector \mathbf{X} as illustrated in Fig. 11.

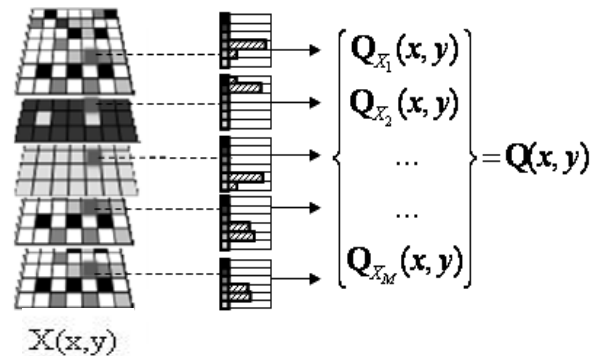


Fig. 11. Quantization of a spectral pixel.

D. Spectral-Spatial Features Integration

To construct the spectral-spatial histogram we need to define a neighborhood around each spectral pixel. In this way, a fuzzy histogram is computed using the quantized vectors \mathbf{Q} that are calculated as illustrated in Fig. 11 for all spectral pixels contained in the neighborhood.

$$\mathbf{H}(x,y) = \sum_{i=x-A/2}^{x+A/2} \sum_{j=y-B/2}^{y+B/2} \mathbf{Q}(i,j) \quad (12)$$

The histogram $H(x,y)$ shown in (12) encodes the spatial distribution for each spectral component X_i inside the selected neighborhood (size $A \times B$) and the spectral characteristics associated with non-ferrous materials are captured by the histogram's shape.

It is useful to note that equation (12) generates the same result as in the case when the fuzzy histogram is calculated

for each channel X_i independently and the resulting spectral histograms are concatenated into a single vector. However, the implementation described in (12) has the advantage that allows the calculation of the histograms for different sized neighborhoods by just performing additive operations. This property is very useful for our implementation since the compound descriptor characterizing two regions would be the same as the sum of the descriptors that are calculated for each region individually. This opens the possibility of real-time implementation for the region merging procedure that will be detailed in Section IV.

III. CLASSIFICATION PROCEDURE

In the previous section, the procedure that is applied to obtain the feature vectors that encompass the spectral and spatial features has been detailed. The histogram vector shown in equation (12) defines the distribution of the spectral information in a pre-defined neighborhood around the pixel (x, y) and is used as input for classification. In our implementation, the multivariate Gaussian classifier is proposed to perform the material classification since the Gaussian distributions approximate well the dispersion of the spectral-spatial feature vectors within each class of non-ferrous materials.

A Gaussian model for each material is created where μ and Σ are the mean vector and the covariance matrix of the modeled class.

$$N(\mathbf{x}|\mu, \Sigma) = \frac{1}{(2\pi)^{D/2}} \frac{1}{|\Sigma|^{1/2}} e^{\left\{-\frac{1}{2}(\mathbf{x}-\mu)^T \Sigma^{-1}(\mathbf{x}-\mu)\right\}} \quad (13)$$

The classification stage is carried out by checking each spectral-spatial vector $H(x,y)$ calculated for each pixel in the image against the normalized distributions that define each material class. Each pixel in the decorrelated hyper-spectral image is labeled to the class that achieves the minimum matching cost.

IV. REGION MERGING

The aim of the first stage classification is to label each pixel in the image with respect to the non-ferrous material classes. Our investigations revealed that due to inter-class overlap some pixels are misclassified. The errors in classification were mostly caused by strong highlights and various oxidization levels encountered for similar materials.



Fig. 12. (a) Classification results obtained when the neighborhood fuzzy histograms are used as input vectors. (b) Classification results obtained after the application of the region merging procedure.

However, in the vast majority of cases the misclassified regions are small and in general they are connected to larger regions that were correctly classified. Based on this observation, a merging procedure for all connected regions is applied and for each region resulting from this process statistics are calculated to solve the misclassifications. Using this approach, the whole connected regions are statistically compared against the class models to decide if a particular region should be re-classified or whether two or more regions should be merged. To achieve this, the fuzzy histogram is calculated for the entire region resulting from the merging process as explained in Section II.D. The histogram merging process is illustrated in equation (14).

$$\mathbf{H}(\Omega) = \sum_{\forall(i,j) \in \Omega} \mathbf{Q}(i,j), \quad \Omega = \cup_{i \in [1,n]} R_i \quad (14)$$

where Ω is the union of the connected regions R_i . By performing region merging, we increase the statistical relevance of the spectral-spatial vector since the merged region is significantly larger than the size of the neighborhood where the spectral-spatial vectors for each pixel in the image were calculated. Figs. 13 and 14 illustrate this process.

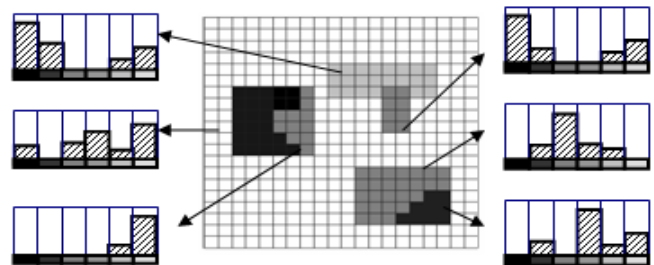


Fig. 13. Extraction of the region histogram for each of the pre-classified regions.

While the histograms depicted in Fig. 13 are calculated from image regions with different sizes, in order to compare them against the Gaussian models constructed for each class they are normalized by dividing each bin of the histogram with the number of elements that form the distribution.

In Fig. 14 each pair of connected regions are checked for merging. To do this, the region histogram is calculated for each region (H_a and H_b) and a joint histogram is calculated for the region obtained after the H_a and H_b regions are merged (H_{merged}).

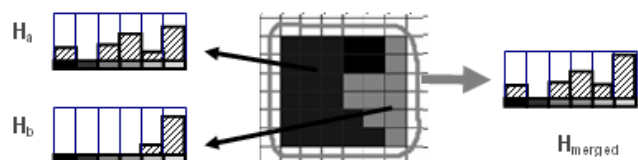


Fig. 14. Histograms of the 2 candidate regions (H_a , H_b) and the histogram of the merged region (H_{merged}).

The H_a , H_b and H_{merged} histograms are checked against the Gaussian models associated with all material classes stored in the database and for each histogram will be assigned a class label in agreement to the class model that minimize the matching cost.

If H_a and H_b are assigned different class labels, the probability for each region to belong to the assigned class is calculated to decide whether the regions should be merged or not. The merging probability is calculated as follows,

$$P(H_i \in C_j) = N(\mathbf{x} | \boldsymbol{\mu}_j, \Sigma_j) \quad (15)$$

The matching cost attained by the merged region H_{merged} (calculated using equation 17) is compared against the matching costs obtained for the two separated regions H_a and H_b (see equation 16).

$$P(H_a \in C_a, H_b \in C_b) = P(H_a \in C_a) \cdot \frac{N_a}{N_{merged}} + P(H_b \in C_b) \cdot \frac{N_b}{N_{merged}} \quad (16)$$

$$P(H_{merged} \in C_{merged}) = N(\mathbf{x} | \boldsymbol{\mu}_{C_{merged}}, \Sigma_{C_{merged}}) \quad (17)$$

To quantify the contribution of each region in equation (16) the matching cost for each region is weighted by the number of elements in each region (N_a and N_b) and the number of elements contained in the merged region (N_{merged}). The regions are merged if the matching cost calculated for H_{merged} is smaller than the matching cost attained for H_a and H_b .

V. RESULTS

The validation of the proposed spectral-spatial method has been carried out in the context of non-ferrous waste material classification. In this investigation the following materials are evaluated: white copper, aluminum, Stainless Steel, brass, copper and lead (see Fig. 15).

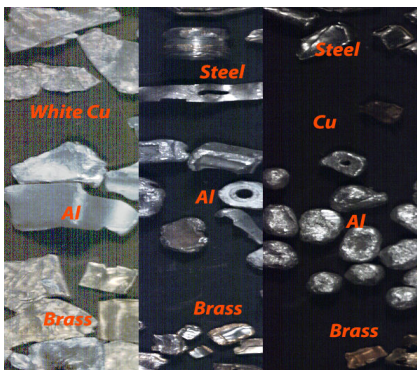


Fig. 15. The non-ferrous materials investigated in this study.

The hyper-spectral data evaluated in our study has been acquired using a PHL Fast10 CL spectral camera manufactured by Specim [11]. Although this camera is able to capture 1024 wavelengths, we elected to capture 80 uniformly distributed wavelengths in the spectral range [384.05nm, 1008.10nm]. The motivation behind this approach is twofold: the reduction of the onerous

computational requirements to capture and process the full resolution hyper-spectral data (1024 wavelengths) and to reduce the problems associated with the construction of high dimensional feature spaces (due to the high correlation between contiguous spectral bands) [46]. The illumination source consists of a mixture of halogen and near ultraviolet lamps that fully cover the analyzed spectrum range. In order to minimize the issues caused by non-even illumination, specular highlights and shadows diffuse light sources were employed.

The developed machine vision system consists of three independent components: the feeding device, conveyor and a part-extractor module. The shredded WEEE mixture is automatically loaded onto a non-specular black conveyor belt (600 mm wide) via a vibratory feeder to ensure that the non-ferrous materials are arranged into a thin layer prior to their arrival at the inspection line that performs the material classification in hyper-spectral data. The conveyor speed was set at 20 m/min and the non-ferrous materials were separated using a pneumatic part-extractor.

The material samples that were used to validate the proposed non-ferrous material classification system have been provided by Indumetal Recycling S.A. and IGE Hennemann Recycling GmbH which are part of the SORMEN project consortium [2]. The non-ferrous materials have been manually sorted by expert operators and in this process they use all the available knowledge about each non-ferrous waste fraction. In this study the captured datasets were divided into training and testing sets where half of the data was used for training and the remaining half was used for testing. From each of these datasets more than 500,000 spectral-spatial descriptors were extracted. The experimental results reported in this paper were only conducted on the testing datasets.

A. Background Removal

In order to remove the background information, a pixel-based evaluation proved to be sufficient to identify the background. For this operation no spectrum normalization was applied since the background does not present specular properties. The background is removed by performing a binary classification where pixel-based Gaussian models are constructed for background and non-ferrous materials. The identification of the background information attained a classification rate of 97%.

B. Data Decorrelation. Classic Approaches and Fuzzy Spectral Energy Response

After removing the background information, the two different decorrelation methods discussed in Section II were tested in order to determine which method generates the best results. In this regard, one of the goals of this investigation was to calculate the optimal number of PCA components and the optimal number of fuzzysets. The experimental results are depicted in Table I.A. In this evaluation the classification has been carried out at pixel-level (using single-pixel spectral features). The data depicted in Table I.A indicates that the best results are

obtained when the number of fuzzysets is selected in the range 8 to 24. Similar results were obtained when the PCA technique has been employed to decorrelate the original hyper-spectral data. The experimental results shown in Table I.A reveal that the RGB data is not sufficient to accurately capture the characteristics associated with non-ferrous materials. In our experiments, when the RGB data was applied for material classification, the correct recognition rate was only 43.83%. The experimental results depicted in Table I.A indicate that the application of the data decorrelation techniques is opportune as the classification results obtained for decorrelated data (number of features >2) are higher than the results obtained for original hyper-spectral data (80 spectral wavelengths) – see the result shown in the last column of Table I.B. For comparative purposes, additional classification results obtained for other decorrelation schemes such as Wavelet decomposition [25], LDA (see Table I.A), and automatic band selection based on floating search method (FSM) [47] (see Table I.B) are included.

TABLE I.A
CLASSIFICATION RESULTS USING SINGLE PIXEL SPECTRAL FEATURES

| Number of features | PCA | Fuzzysets | Wavelet | RGB | LDA |
|--------------------|--------|-----------|---------|--------|--------|
| 2 | 53.08% | 52.76% | 51.05% | | |
| 4 | 61.40% | 63.10% | 53.96% | | |
| 8 | 66.43% | 71.52% | 63.79% | 43.83% | 62.86% |
| 16 | 64.11% | 71.43% | 69.59% | | |
| 24 | 67.95% | 71.67% | 68.69% | | |

TABLE I.B
CLASSIFICATION RESULTS USING SINGLE PIXEL SPECTRAL FEATURES.
AUTOMATIC BAND SELECTION (FLOATING SEARCH METHOD) AND
UNPROCESSED (RAW) SPECTRAL DATA

| Number of spectral bands | Floating search method (FSM) | Original (raw) spectral data (80 wavelengths) |
|--------------------------|------------------------------|---|
| 2 | 44.84% | |
| 4 | 59.86% | |
| 8 | 62.03% | |
| 16 | 55.67% | |
| 24 | 66.95% | |
| 80 | | 55.67% |

The experimental results depicted in Tables I.A and I.B reveal that the spectrum fuzzyfication and the classical data decorrelation methods (PCA, LDA, Wavelet and automatic band selection) produced promising results when applied to the decorrelation of hyper-spectral data. However, in our experiments the proposed fuzzysets outperformed these techniques and at the same time our approach avoids the complications associated with the training procedure required by classic data decorrelation methods that were analyzed in this study. For these reasons, the technique based on fuzzysets was deemed as the most appropriate decorrelation method. Fig. 16 illustrates the results returned by the pixel-based classification approach when applied to hyper-spectral data that was decorrelated using 8 fuzzysets.

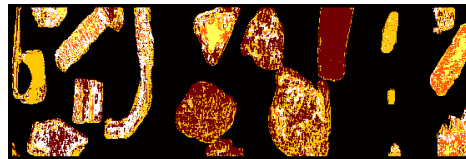


Fig 16. Pixel-based classification results when applied to decorrelated hyper-spectral data (8 fuzzysets).

C. Neighborhood Fuzzy Histograms

In the experiments described in the previous section, the spatial information was not included in the process of modeling the non-ferrous material characteristics. In order to include the spatial information in the construction of the feature vectors, fuzzy spatial histograms are calculated for each pixel in the image data as explained in Section II.D. To evaluate the contribution of the spatial information in the classification process, the spectral-spatial vectors (fuzzy spatial histograms) are constructed for differing window sizes. The classification process is carried out using the multivariate Gaussian classifier that has been detailed in Section III. The experimental results are depicted in Table II.

TABLE II
CLASSIFICATION RESULTS USING FUZZY HISTOGRAMS CALCULATED IN
NEIGHBORHOODS OF DIFFERING SIZES

| Window Size | PCA 8 features | Fuzzysets 8 features | Wavelet 8 features | FSM 8 bands | RGB |
|-------------|----------------|----------------------|--------------------|-------------|--------|
| 3×3 | 67.19% | 77.30% | 67.68% | 71.24% | 53.03% |
| 5×5 | 73.77% | 81.48% | 72.48% | 75.35% | 56.14% |
| 7×7 | 76.42% | 83.77% | 76.53% | 76.84% | 56.46% |
| 11×11 | 78.85% | 85.62% | 78.34% | 79.14% | 57.76% |
| 15×15 | 79.34% | 86.45% | 79.15% | 80.68% | 59.21% |
| 19×19 | 80.41% | 86.63% | 80.85% | 80.74% | 59.83% |
| 23×23 | 81.32% | 86.42% | 81.10% | 83.78% | 59.90% |

The experimental data shown in Table II indicates that the development of compound feature vectors that encompass the spectral and spatial information generates more robust image descriptors that are able to sample in a more elaborate fashion the spectral characteristics of the non-ferrous materials. The results depicted in Table II prove that the decorrelation technique based on spectrum fuzzyfication produces more consistent results than PCA, Wavelet decomposition and the selection of the most discriminant bands for all window sizes and they also demonstrate that the RGB data is not suitable for non-ferrous material classification. Based on the experimental data shown in Table II it can be concluded that the application of the spectral-spatial vectors for material classification proved to be opportune since the overall classification rate is increased to over 86%. An experimental example is depicted in Fig. 17.

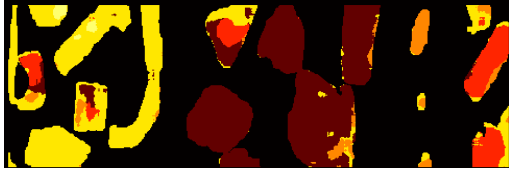


Fig. 17. Classification results using spectral-spatial feature vectors.

D. Region Merging

The regions identified after the application of the neighborhood (spectral-spatial) histograms (see Section V.C) are subjected to re-classification using the procedure discussed in Section IV. In this process for each connected region the merging cost is evaluated using the equations (15) and (16) and the merging decisions are based on the minimization of the matching cost criterion. The experimental results shown in Table III indicate that optimal results are obtained when the spectral-spatial histograms are calculated in a 7×7 neighborhood.

TABLE III
CLASSIFICATION RESULTS AFTER REGION MERGING

| Window Size | PCA 8 features | Fuzzysets 8 features | Wavelet 8 features | FSM 8 bands |
|-------------|-------------------|-------------------------|-----------------------|----------------|
| 3×3 | 75.16% | 96.18% | 94.18% | 94.76% |
| 5×5 | 93.17% | 96.67% | 96.13% | 93.51% |
| 7×7 | 94.44% | 98.36% | 96.02% | 93.81% |
| 11×11 | 92.84% | 98.36% | 95.65% | 91.34% |
| 15×15 | 92.59% | 98.36% | 95.75% | 90.86% |
| 19×19 | 92.89% | 96.94% | 94.75% | 90.93% |
| 23×23 | 92.51% | 96.94% | 94.68% | 90.41% |

The results depicted in Table III show that the application of the region merging process reduced to a great extent the level of misclassified regions.

TABLE IV
CONFUSION MATRIX CALCULATED FOR ALL NON-FERROUS MATERIAL CLASSES
(PROPOSED REGION-BASED CLASSIFICATION APPROACH)

| Real \ Classified | AL | Copper | Brass | Lead | Steel | White Copper |
|-------------------|-------|--------|-------|-------|--------|--------------|
| AL | 97.58 | 0.00 | 0.00 | 0.00 | 0.00 | 0.00 |
| Copper | 0.00 | 98.39 | 0.00 | 0.00 | 0.00 | 0.00 |
| Brass | 0.00 | 0.00 | 96.90 | 0.00 | 0.00 | 0.00 |
| Lead | 0.02 | 0.00 | 0.00 | 98.89 | 0.00 | 0.00 |
| Steel | 2.39 | 1.61% | 3.10 | 1.11 | 98.41 | 0.00 |
| White Copper | 0.00 | 0.00 | 0.00 | 0.00 | 1.59 | 100.00 |
| Overall | | | | | 98.36% | |

The confusion matrix (Table IV) constructed for all materials evaluated in this study reveals that most errors are caused by the misclassification of the Stainless Steel and the class overlap generated by non-ferrous materials with similar spectral properties. Additional experimental results are depicted in Figs. 18 and 19.



Fig. 18. Classification results after the image depicted in Fig. 16 has been subjected to region merging and re-classification.

To illustrate the appropriateness of the proposed spectral-spatial features, in Table V results that illustrate the improvement in performance when the classification is performed using single-pixel spectral descriptors, fuzzy histograms and after region merging are depicted. (To limit the size of the table only the results obtained when the fuzzy histograms are calculated in a 7×7 neighborhood are reported).

TABLE V
COMPARATIVE RESULTS: SINGLE-PIXEL DESCRIPTORS, FUZZY
HISTOGRAMS AND REGION MERGING

| Algorithm | PCA 8 features | Fuzzysets 8 features | Wavelet 8 features | FSM 8 bands |
|------------------|-------------------|-------------------------|-----------------------|----------------|
| Single pixel | 66.43% | 71.52% | 63.79% | 62.03% |
| Fuzzy histograms | 78.85% | 85.62% | 76.53% | 79.14% |
| Region merging | 94.44% | 98.36% | 96.02% | 93.81% |

Another set of experiments was performed to evaluate the computational cost associated with the developed material classification algorithm and the experimental results are depicted in Table VI. These experiments have been conducted using a Pentium 2.33 GHz PC, 2 GB RAM memory and running Windows XP. Currently, we investigate different computational architectures that will further reduce the computational overhead associated with the proposed classification scheme.

TABLE VI
COMPUTATIONAL COST ASSOCIATED WITH THE DEVELOPED MATERIAL
CLASSIFICATION ALGORITHM. IN THESE EXPERIMENTS THE HYPER-
SPECTRAL DATA HAS BEEN DECORRELATED USING 8 SPECTRAL FUZZYSETS

| Window Size | Time per pixel (ms) |
|-------------|---------------------|
| 1×1 | 0.0004557 |
| 5×5 | 0.0005733 |
| 7×7 | 0.0007497 |
| 11×11 | 0.0012643 |
| 15×15 | 0.0020287 |
| 19×19 | 0.0029872 |

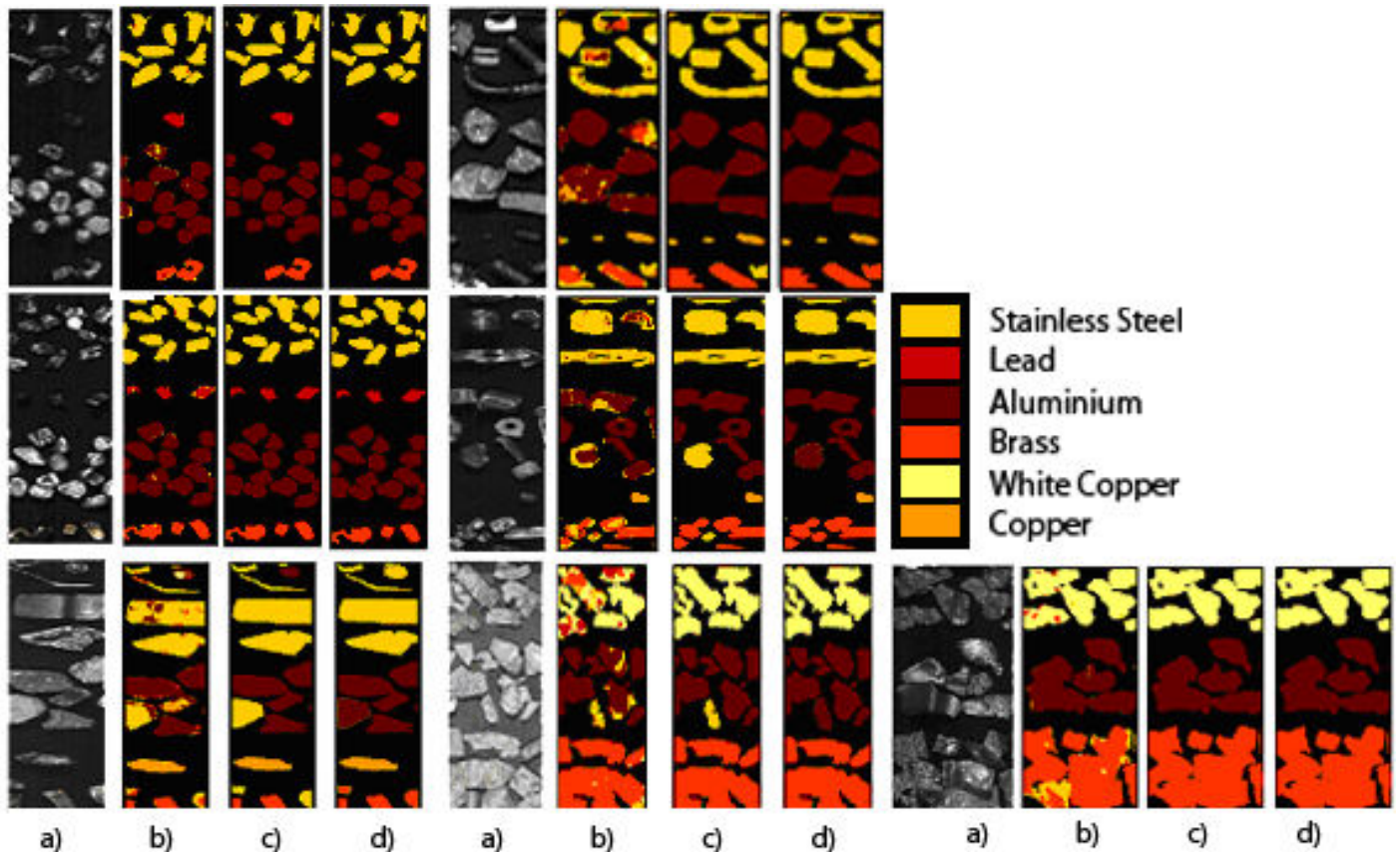


Fig. 19. Additional classification results. (a) Original image. (b) Fuzzy histogram-based classification results. (c) Results after region merging and re-classification. (d) Ground-truth image.

VI. CONCLUSIONS

The aim of this paper was to detail the theoretical and practical issues associated with the implementation of an integrated system for non-ferrous material sorting. In our approach, the developed FUSSE algorithm addressed issues related to the decorrelation of hyper-spectral data using an approach that emulates the human visual system and the development of fuzzy histograms that integrates the spectral and spatial features in a compact descriptor that is able to accurately sample the properties of the non-ferrous materials. The proposed approach avoids the requirement of complex and subjective training procedures and at the same time allows the construction of elaborate statistical models that can be applied for robust non-ferrous material classification. To further improve the classification results, we have devised a region merging post-processing scheme that is applied to re-classify the connected regions in agreement with the minimization of a matching cost criterion.

In this study a large number of experiments have been conducted to evaluate the efficiency of the proposed system. In this regard, the experimental data reported in this paper indicates that the unprocessed (raw) hyper-spectral information is not suitable to accurately capture the characteristics of the non-ferrous materials. Our experiments revealed that significant improvements are obtained when the material classification is performed on

decorrelated hyper-spectral data. Another key issue related to the implementation of the material-sorting algorithm described in this paper resides in the integration of the spatial and spectral features in a compact image descriptor. The experimental data clearly demonstrate that considerably improved results are obtained when the characteristics of the analyzed non-ferrous materials are modeled using the proposed fuzzy spectral histograms to achieve spatial feature integration. The non-ferrous material classification (FUSSE) algorithm attained over 98% correct classification when applied to the identification of the WEEE scraps containing six different non-ferrous materials (white copper, aluminium, Stainless Steel, brass, copper and lead).

The experimental results indicate that most errors are caused by the misclassification of the Stainless Steel. To reduce the rate of misclassification associated with this material, future work will be concentrated on the development of multi-resolution classification schemes that will be applied to increase the discriminative power of the proposed spectral-spatial features. Additional future work will also explore the feasibility of implementing the proposed classification algorithm on a hardware platform in order to achieve the computational speed required for real-time operation and to investigate the application of multiple narrow-band illumination arrangements to improve the discrimination between the Stainless Steel and the other non-ferrous materials with similar spectral properties.

ACKNOWLEDGMENTS

We would like to thank Robotiker-Tecnalia, Specim and SORMEN project consortium for providing the data and the non-ferrous materials that have been used in the validation of the proposed algorithm.

Part of this work was carried out while Artzai Picón was a visiting researcher in the Centre for Image Processing and Analysis (CIPA), Dublin City University from February 2007 to February 2008.

REFERENCES

- [1] Directive 2002/96/EC of the European Parliament and of the Council of 27 January 2003 on waste electrical and electronic equipment (WEEE) - Joint declaration of the European Parliament, the Council and the Commission relating to Article 9.
- [2] SORMEN - Innovative Separation Method for Non Ferrous Metal Waste from Electric and Electronic Equipment (WEEE) based on Multi- and Hyperspectral Identification project, Sixth Framework Programme Horizontal Research Activities Involving SMES Co-Operative Research, 2006, <http://www.sormen.org/>
- [3] A. Bereciartua, and J. Echazarra, "Sistema basado en identificación multiespectral para la separación de metales no férricos en WEEE en logística inversa", *1er Congreso de Logística y Gestión de la Cadena de Suministro*, 2007.
- [4] D.B. Spencer, "The high-speed identification and sorting of nonferrous scrap", *JOM Journal of the Minerals, Metals and Materials Society*, vol. 57, no. 4, pp. 46-51, 2005.
- [5] M. Kutila, J. Viitanen, and A. Vattulainen, "Scrap metal sorting with colour vision and inductive sensor array", *Computational Intelligence for Modelling, Control and Automation*, pp. 725-729, Vienna, Austria, 2005.
- [6] E.J. Sommer, C.E. Ross, and D.B. Spencer, *Method and apparatus for sorting materials according to relative composition*, US Patent 7,099,433, 2006.
- [7] D.A. Wahab, A. Hussain, E. Scavino, M. Mustafa, and H. Basri, "Development of a prototype automated sorting system for plastic recycling", *American Journal of Applied Sciences*, vol. 3, no. 7, pp. 1924-1928, 2006.
- [8] A.J. Gesing, "ELVs: How they fit in the global material recycling system and with technologies developed for production or recycling of other products and materials", *6th International Automobile Recycling Congress*, Amsterdam, Netherlands, 2006
- [9] C.I. Chang, *Hyperspectral Imaging: Techniques for Spectral Detection and Classification*, Kluwer Academic Publishers Group, ISBN:0-306-47483-5, 2003.
- [10] B. Tso, and R.C. Olsen, "Scene Classification Using Combined Spectral, Textural and Contextual Information", SPIE, ATMHUI X, 2004.
- [11] Specim Spectral Imaging Ltd. <http://www.specim.fi/>
- [12] Z. Pan, G. Healey, M. Prasad, B. Tromberg "Face Recognition in Hyperspectral Images", *IEEE Transactions on Pattern Analysis and Machine Intelligence*, vol. 25, no. 12, pp. 1552-1560, 2003
- [13] D. Naso, B. Turchiano, and P. Pantaleo, "A fuzzy-logic based optical sensor for online weld defect-detection", *IEEE Transactions on Industrial Informatics*, vol. 1, no. 4, pp. 259-273, 2005.
- [14] H. Grahn and P. Geladi (Eds.), *Techniques and Applications of Hyperspectral Image Analysis*, Wiley, ISBN-10: 0-470-01086-X, 2007
- [15] D. Slater, and G. Healey, "Material classification for 3D objects in aerial hyperspectral images", *IEEE Computer Society Conference on Computer Vision and Pattern Recognition (CVPR'99)*, vol. 2, pp. 2262-2267, 1999.
- [16] G. Healey, and D. Slater, "Models and methods for automated material identification in hyperspectral imagery acquired under unknown illumination and atmospheric conditions", *IEEE Transactions on Geoscience and Remote Sensing*, vol. 37, no. 6, pp. 2706-2717, 1999.
- [17] N. Keshava, "Distance metrics and band selection in hyperspectral processing with application to material classification and spectral libraries", *IEEE Transactions on Geoscience and Remote Sensing*, vol. 42, no. 7, pp. 1552-1565, 2004.
- [18] C. Willis, "Hyperspectral image classification with limited training data samples using feature subspaces", *Algorithms and Technologies for Multispectral, Hyperspectral and Ultraspectral Imagery X*, SPIE, 2004.
- [19] G. Acciani, G. Brunetti, and G. Fornarelli, "Application of neural networks in optical inspection and classification of solder joints in surface mount technology", *IEEE Transactions on Industrial Informatics*, vol. 2, no. 3, pp. 200-209, 2006.
- [20] B.K. Feather, S.A. Fulkerson, J.H. Jones, R.A. Reed, M. Simmons, D. Swann, W.E. Taylor, and L.S. Bernstein, "Compression technique for plume hyperspectral images", *Algorithms and Technologies for Multispectral, Hyperspectral and Ultraspectral Imagery XI*, SPIE, 2005
- [21] C.Y. Kuan, and G. Healey, "Band selection for recognition using moment invariants", *Algorithms and Technologies for Multispectral, Hyperspectral and Ultraspectral Imagery XI*, SPIE, 2005.
- [22] S. Perkins, K. Edlund, D. Esch-Mosher, D. Eads, N. Harvey, and S. Brumby, "Genie Pro: Robust image classification using shape, texture and spectral information", *Algorithms and Technologies for Multispectral, Hyperspectral and Ultraspectral Imagery XI*, SPIE, 2005.
- [23] D. Manolakis, and D. Marden, "Dimensionality reduction of hyperspectral imaging data using local principal component transforms", *Algorithms and Technologies for Multispectral, Hyperspectral and Ultraspectral Imagery X*, SPIE, 2004.
- [24] P. Tatzer, M. Wolf, and T. Panner, "Industrial application for inline material sorting using hyperspectral imaging in the NIR range", *Real-Time Imaging*, vol. 11, no. 2, Spectral Imaging II, pp. 99-107, 2005
- [25] P. Kempeneers, S. De Backer, W. Debruyne, P. Coppin, and P. Scheunders, "Generic Wavelet-Based Hyperspectral Classification Applied to Vegetation Stress Detection", *IEEE Transactions on Geoscience and Remote Sensing*, vol. 43, no. 3, pp. 610-614, 2005.
- [26] J. Wang, and C.I. Chang, "Independent component analysis-based dimensionality reduction with applications in hyperspectral image analysis", *IEEE Transactions on Geoscience and Remote Sensing*, vol. 44, no. 6, pp. 1586-1600, 2006.
- [27] H. Kwon, S.Z. Der, N.M. Nasrabadi, and H. Moon, "Use of hyperspectral imagery for material classification in outdoor scenes", *SPIE Proceedings Series, Algorithms, Devices, and Systems for Optical Information Processing III*, vol. 3804, Denver, USA, pp. 104-115, 1999.
- [28] B. Guo, R.I. Damper, S.R. Gunn, and J.D.B. Nelson, "A fast separability based feature-selection method for high-remotely sensed image classification", *Pattern Recognition*, vol. 41, pp. 1653-1662, 2008.
- [29] J.M. Geusebroek, R. Boomgaard, A.W.M. Smeulders, and H. Geerts "Color invariance", *IEEE Transactions on Pattern Analysis and Machine Intelligence*, vol. 23, no. 12, pp. 1338-1350, 2001.
- [30] D. Manolakis, C. Siracusa, and G. Shaw, "Hyperspectral subpixel target detection using the linear mixing model," *IEEE Transactions on Geoscience and Remote Sensing*, vol. 39, no. 7, pp. 1392-1409, 2001.
- [31] J. Broadwater, and R. Chellappa, "Hybrid detectors for subpixel targets" *IEEE Transactions on Pattern Analysis and Machine Intelligence*, vol. 29, no. 11, pp. 1891-1903, 2007.
- [32] G. Mercier, and M. Lennon, "On the characterization of hyperspectral texture", *IEEE International Geoscience and Remote Sensing Symposium (IGARSS'02)*, vol. 5, pp. 2584-2586, 2002.
- [33] G. Rellier, X. Descombes, J. Zerubia, and F. Falzon, "A Gauss-Markov Model for hyperspectral texture analysis of urban areas", *16th International Conference on Pattern Recognition (ICPR'02)*, vol. 1, pp. 692-695, 2002.
- [34] B. Ramakrishna, J. Wang, C. Chang, A. Plaza, H. Ren, C.C. Chang, J.L. Jensen, and J.O. Jensen, "Spectral/spatial hyperspectral image compression in conjunction with virtual dimensionality", *Algorithms and Technologies for Multispectral, Hyperspectral and Ultraspectral Imagery XI*, SPIE, 2005.

- [35] S. Shafer, "Using color to separate reflection components", *Color Research and Applications*, vol. 10, pp. 210-218, 1985
- [36] R.T. Tan, K. Nishino, and K. Ikeuchi, "Separating reflection components based on chromaticity and noise analysis", *IEEE Transactions on Pattern Analysis and Machine Intelligence*, vol. 26, no. 10, pp. 1373-1379, 2004.
- [37] H. Stockman, and T. Gevers, "Detection and Classification of Hyper-Spectral Edges", *Proc. 10th British Machine Vision Conference (BMVC)*, 1999.
- [38] A. Gorban, B. Kegl, D. Wunsch, and A. Zinovyev (Eds.), "Principal Manifolds for Data Visualization and Dimension Reduction", LNCS 58, Springer, ISBN 978-3-540-73749-0, 2007.
- [39] C.M. Bishop, *Pattern Recognition and Machine Learning*, Springer, ISBN-10: 0-387-31073-8, 2006.
- [40] H. Kwon, and N.M. Nasrabadi, "Kernel matched subspace detectors for hyperspectral target detection", *IEEE Transactions on Pattern Analysis and Machine Intelligence*, vol. 28, no. 2, pp. 178-194, 2006.
- [41] S. Abe, and M.S. Lan, "A method for fuzzy rules extraction directly from numerical data and its application to pattern classification", *IEEE Transactions on Fuzzy Systems*, vol. 3, no. 1, pp. 18-28, 1995.
- [42] M.R. Emami, I.B. Turksen, and A. Goldenberg, "Development of a fuzzy systematic methodology of fuzzy logic modeling", *IEEE Transactions on Fuzzy Systems*, vol. 6, no. 3, pp. 346-361, 1998.
- [43] A.M. Martinez, and A.C. Kak, "PCA versus LDA", *IEEE Transactions on Pattern Analysis and Machine Intelligence*, vol. 23, no. 2, pp. 228-233, 2001.
- [44] P. Comon, "Independent Component Analysis: a new concept?", *Signal Processing*, vol. 36, no. 3, pp. 287-314, 1994.
- [45] C.I. Chang, *Hyperspectral data exploitation: theory and applications*, pp. 227, Wiley, 2007.
- [46] S.J. Sangwine, and R.E.N. Horne, *The Colour Image Processing Handbook*, ISBN 0412806207, Springer, 1998.
- [47] P. Pudil, J. Novovicova, and J. Kittler, "Floating search methods in feature selection", *Pattern Recognition Letters*, vol. 15, no. 11, pp. 1119-1125, 1994.



Artzai Picón received the M.Eng degree in Industrial Engineering (2002), and M.Res degree in Automatics Electronics and Control (2005) and PhD (2009) from the University of the Basque Country, Spain. During the period 2000-2002, he collaborated with the Computer Image Processing Group (GTI2) in the Department of Systems Engineering and Automatics. Since then, he has been working as a Researcher for Tecnalia Research Corporation where he has been involved in over 30 research projects. His research interests include image classification and segmentation and the application of these technologies to industrial tasks. In 2002 he received the Best M.Eng. Final Project Award from Accenture Company for the implementation of a facial recognition system and in 2006 he received the ONCE International Research and Development Award in New Technologies for The Blind and Visually Impaired.



Ovidiu Ghita received the BE and ME degrees in Electrical Engineering from Transilvania University Brasov, Romania and the Ph.D. degree from Dublin City University, Ireland. From 1994 to 1996 he was an Assistant Lecturer in the Department of Electrical Engineering at Transilvania University. Since then he has been a member of the Vision Systems Group at Dublin City University (DCU) and currently he holds a position of DCU-Research Fellow. Dr. Ghita has authored and co-authored over 70 peer-reviewed research papers in areas of instrumentation, range acquisition, machine vision, texture analysis and medical imaging.



Paul F. Whelan (S'84-M'85-SM'01) received his B.Eng. (Hons) degree from NIHED, M.Eng. from the University of Limerick, and his Ph.D. (Computer Vision) from the University of Wales, Cardiff, UK (Cardiff University). During the period 1985-1990 he was employed by Industrial and Scientific Imaging Ltd and later Westinghouse (WESL), where he was involved in the research and development of high speed computer vision systems. He was appointed to the School of Electronic Engineering, Dublin City University (DCU) in 1990 and is currently Professor of Computer Vision (Personal Chair). Prof. Whelan founded the Vision Systems Group in 1990 and the Centre for Image Processing & Analysis in 2006 and currently serves as its director.

As well as publishing over 150 peer reviewed papers, Prof. Whelan has co-authored 2 monographs and co-edited 3 books. His research interests include image segmentation, and its associated quantitative analysis with applications in computer/machine vision and medical imaging. He is a Senior Member of the IEEE, Fellow of IET, Chartered Engineer and a member of IAPR. He served as a member of the governing board (1998-2007) of the *International Association for Pattern Recognition* (IAPR), a member of the *International Federation of Classification Societies* (IFCS) council and President (1998-2007) of the *Irish Pattern Recognition and Classification Society* (IPRCS). Prof. Whelan is a HEA-PRTLI (RINCE, NBIP) funded principal investigator.



Pedro M. Iriondo received the degree in Industrial Engineering in 1981 and began his professional activity working in different companies. In 1986 he founded the company *Adicorp* dedicated to the research, integration and development of industrial vision systems.

In 2001 he received the Ph.D. degree in Industrial Engineering - Electronics and Control Engineering - from the University of the Basque Country UPV-EHU, Spain. Since 1989 he has been an Assistant Professor with the Department of Automatic Control and Systems Engineering, ETSI of Bilbao, University of the Basque Country UPV-EHU. Currently, he is the Assistant Director of the School of Engineering of Bilbao responsible for relations with private companies. His research interest is focused in the fields of image processing, face detection and recognition, image transmission and stochastic systems.